CrossMark

Laboratory tests and numerical simulations on the impact of subsurface barriers to saltwater intrusion

Fu-lin Li[1] · Xue-qun Chen[1] · Cai-hong Liu[1] · Yan-qing Lian[2] · Li He[1]

Abstract Subsurface barriers have been used as one of the engineering measures to prevent saltwater intrusion in the coastal aquifers in China. However, the effectiveness of those barriers has not been studied thoroughly. In this research, comparative studies using sandbox test as a physical model and the FEFLOW-based groundwater numerical model were conducted for better understanding of the dynamic processes of saltwater intrusion with and without subsurface barriers. Both laboratory tests and numerical simulation without subsurface barriers showed that the saltwater front intruded to 18, 55 and 63 in the aquifer in 10, 20 and 40 min, respectively. The impact of the different permeability of the subsurface barriers to the migration distance and diffusion of saltwater front was also tested in the laboratory and simulated by using the two-dimensional numerical model. Results showed the saltwater front could still pass through the subsurface barrier and continued moving forward when the permeability K of the subsurface barriers was 9.9×10^{-7} m/s. When the K of the subsurface barriers was 1.3×10^{-7} m/s, the salt–front passed through the subsurface barrier in 40 min, and the migration rate of the salt–fresh water interface did not change in 70 min. When the K was 3.7×10^{-8} m/s, the saltwater front could not go through the subsurface barriers. These research results indicated that the subsurface barriers with low permeability ($K = 3.7 \times 10^{-8}$ m/s) could prevent the saltwater intrusion effectively. The results of this case study provide important practical significance for the prevention of saltwater intrusion in coastal areas.

Keywords Saltwater intrusion · Subsurface barriers · Sandbox test · FEFLOW

✉ Cai-hong Liu
caihongliu1988@sina.com

[1] Water Resources Research Institute of Shandong Province, Jinan 250013, Shandong Province, China

[2] University of Illinois at Urbana-Champaign, Urbana-Champaign, USA

1 Introduction

Seawater intrusion constitutes a prominent hydrological problem in many coastal areas of the world (Lu et al. 2013). A large quantity of groundwater is extracted to meet the needs of agricultural and industrial development and other activities. The overexploitation groundwater of coastal aquifer is the essential reason of seawater intrusion, which contaminates freshwater resources in coastal aquifers by increasing the salinity levels of the groundwater (Zhang et al. 2015). A significant decline of groundwater level caused by groundwater over-exploitation destroyed the water dynamic balance between seawater and freshwater, which caused the freshwater and seawater boundary moves toward inland (Abarca et al. 2007). The seawater intrusion which was universality and destruction has caused common concern. It threatens groundwater resources as well as the ecological environment (Yuan and Liang 2001), such as deterioration of water quality, soil salinization and industrial equipment corrosion. At the same time, endemic disease became serious in the seawater intrusion areas (Allow 2012). Seawater intrusion has become an important factor that restricts the economic and social development of the coastal areas. Therefore, the prevention of seawater intrusion has become an urgent problem to be solved.

Due to the practical importance, the laboratory experiments and numerical modeling of seawater intrusion have attracted remarkable attention, and a lot of valuable results were got in the last decades. At the same time, many simulation models, such as FEMWATER (Lin et al. 1997) and SEAWAT (Guo and Bennett 1998; Guo and Langevin 2002; Abd-Elhamid and Javadi 2011) have been used to simulate and predict seawater intrusion trends in coastal aquifers. Rumer and Harleman (1963) studied the migration rate of salt–fresh water interface in different porous media with a laboratory model of a two-dimensional. Tang et al. (1998) predicted transition zone by electrical conductivity method and then analyzed dynamic characteristics of the transition zone through large-scale advection–dispersion sandbox test. Zhang (2005) analyzed the influence of tide, water level and concentration on the seawater intrusion through laboratory experiment with glass beads as aquifer porous media. Galeati et al. (1992) proposed the variable density unconfined aquifer model to study the seawater intrusion in the south of Italy. Li and Chen (1995) established the three-dimensional finite element model considering density, head and concentration by artificial diffusion-weighted method, and the seawater intrusion in Weizhou Island was studied with the model. Wu et al. (1996) set up the reflect-rock cation exchange mathematical model of seawater intrusion and applied it to simulate the process of ion exchange process of seawater intrusion in Longkou city. Cheng (1999) established a mathematical model of three-dimensional variable density advection–dispersion model to study the migration of salt–fresh water interface in the middle and lower reaches of Yantai Jia River. Chen et al. (2000) derived the solute migration dispersion equation combined with water dynamic and chemistry dynamic in the process of seawater intrusion to solve three-dimensional model of solute transport with high concentration. Saltwater intrusion in coastal aquifers in Goksu Deltaic Plain of Turkey was modeled in three dimensions by Cobaner et al. (2012) with SEAWAT. 3D seawater intrusion model was developed by Chekirbane et al. (2015) for simulating the historical trends of saltwater distribution in coastal aquifers in northeast of Tunisia and predicting its future dynamics under some proposed countermeasures for remediation. Zhao et al. (2016) constructed a three-dimensional (3D) density-dependent numerical model to simulate the seawater intrusion process in heterogeneous coastal aquifers in Zhoushuizi district of the metropolitan Dalian City, and the model was applied to

predict the dynamics and trend of seawater intrusion for the following 30 years from 2010 to 2040 under different rainfall scenarios.

Many researches have been carried out on seawater intrusion in China and abroad, so far, there are two kinds of methods mainly to control the intrusion of seawater, one is to arrange a row of pumping or injection wells along the coastline to discharge and recharge water (Todd 1980), and another method is to pour the impervious curtain to block the seawater (subsurface barrier). Subsurface barrier was first proposed in early twentieth century for the construction of underground reservoirs for saving of groundwater. It refers to the construction of a semipermeable or impermeable structure constructed to intercept the underground runoff, not only to avoid the loss of groundwater, but also to prevent the intrusion of seawater (Allow 2012). There has been a lot of successful practice in the construction of subsurface barrier. Since Japan built subsurface barrier to prevent seawater intrusion, also other subsurface barriers had been built in China, and the saltwater intrusion laboratory experiment and research of subsurface barriers had been carried out.

Subsurface barrier is an engineering measurement for the prevention of saltwater intrusion and has many demonstration projects in China. However, there are fewer researches on subsurface barrier anti-seepage efficiency especially laboratory simulation experiment and the numerical method to simulate the effect of the subsurface barriers to prevent saltwater intrusion. So the objectives of this study are to: (1) simulate saltwater intrusion process without subsurface barriers ($K = 2.2 \times 10^{-3}$ m/s) and with different permeability coefficient subsurface barriers ($K = 9.9 \times 10^{-7}$, 1.3×10^{-7} and 3.7×10^{-8} m/s) by sandbox test in laboratory, (2) evaluate the efficiency of these subsurface barriers to prevent seawater intrusion, (3) numerically simulate the saltwater intrusion in different laboratory test scenarios using FEFLOW model.

2 Methodology

2.1 Laboratory test

In this study, sandbox model experiments were conducted to simulate dynamic characteristics of saltwater interface in porous media. The sandbox was made of transparent organic glass with a length of 180 cm, width of 10 cm and height of 60 cm, and the Markov bottle with freshwater and colored saltwater at both sides is used as supplementary source to keep a continuous flow and the constant water head during the experiment. Adjusting the height of the device to keep the water-level difference between saltwater and freshwater was 30 mm. Glass beads with an average diameter of 0.6–0.9 mm served as porous media in sandbox; multiparous lucite plate with 28 mesh sieve was used to separate glass beads from the saltwater and freshwater and ensure the hydraulic connection. There was a waterproof board between the sand and saltwater area until the experiment began. Two rubber pipes were connected to the outlet of the constant water head device.

The NaCl solution with the concentration of 25 g/L was used to simulate saltwater, and carmine with the concentration of 0.5 g/L was used as colored tracer. There are three reasons we used the carmine with the concentration of 0.5 g/L as colored tracer, first is that the carmine has no adsorption effect on aquifer medium, second is that it will not affect the detection of chloride ions, and sodium chloride will not affect the detection of carmine, and the third is that carmine can migrate with Cl$^-$ at the same rate in the test medium. Fine screens of different aperture were used to simulate subsurface barriers. Subsurface barrier was 28 cm away from the saltwater. The experiment apparatus is shown in Fig. 1.
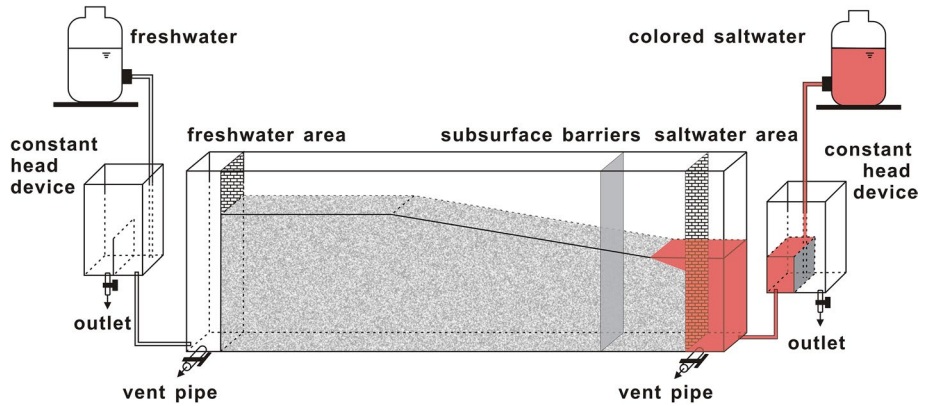
Fig. 1 The sandbox model used to simulate saltwater intrusion

In this study, four scenarios of experiments were performed:

1. Salt water intrusion simulation under nature condition (without subsurface barriers).
2. The anti-seepage board as subsurface barrier was inserted into the sandbox to simulate saltwater intrusion. Three different permeability coefficient subsurface barriers were simulated, which were 9.9×10^{-7}, 1.3×10^{-7} and 3.7×10^{-8} m/s.

One observation point was set after the subsurface barrier.

2.2 Mathematical model

As there are concentration and density difference and transition zone between seawater and freshwater, the simulation model is heterogeneous advection–dispersion model that considering the change of concentration and density, the transition zone and the influence of concentration on fluid velocity. The variable density flow equation of three-dimensional was described as follows (Huyakorn et al. 1987):

$$\frac{\partial}{\partial x_i}\left[K_{ij}\left(\frac{\partial h}{\partial x_j} + \eta c e_j\right)\right] = S_s\frac{\partial h}{\partial t} + \emptyset\eta\frac{\partial c}{\partial t} - \frac{\rho}{\rho_0}q \quad (i, j = 1, 2, 3) \tag{1}$$

where K_{ij} is hydraulic conductivity tensor; h is the reference hydraulic head; x_j $(i, j = 1, 2, 3)$ is Cartesian coordinates; η is density coupling coefficient; c is solute concentration; e_j is the jth component of the gravitational unit vector; S_s is specific storage; t is time; $\emptyset$ is porosity; q is the volumetric flow rate of sources or sinks per unit volume of aquifer; and ρ, ρ_0 is density of mixed water and freshwater.

Assuming that coordinate system is vertical for the convenience of calculation ($e_1 = e_3 = 0$, $e_2 = 1$), the reference water head and density coupling coefficient are defined as:

$$h = \frac{p}{\rho_0 g} + Y \tag{2}$$

$$\eta = \frac{\varepsilon}{C_s} \tag{3}$$

$$\varepsilon = \frac{\rho_s - \rho_0}{\rho_0} \tag{4}$$

where p is fluid pressure; g is gravitational acceleration; Y is the elevation above datum; ε is the density difference ratio; and C_s is the solute concentration corresponding to the maximum density ρ_s.

Hydraulic conductivity is related to the fluid density and viscosity and is defined as:

$$K_{ij} = \frac{k_{ij}\rho g}{\mu} \tag{5}$$

where K_{ij} is intrinsic hydraulic conductivity tensor, and μ is the dynamic viscosity of fluid.

Assuming μ is constant and is equal to the viscosity of freshwater μ_0 and in the meanwhile considering density is a linear function of concentration, so the density of the liquid is described as:

$$\rho = \rho_0 \left(1 + \frac{\varepsilon c}{c_s}\right) \tag{6}$$

The advective–dispersive equation to describe the salt transport is written as (Huyakorn et al. 1987):

$$\frac{\partial}{\partial x_i}\left(D_{ij}\frac{\partial c}{\partial x_j}\right) - V_i\frac{\partial c}{\partial t} = \emptyset\frac{\partial c}{\partial t} + q(c - c^+) \tag{7}$$

$$V_i = -K_{ij}^0\left[\frac{\partial h}{\partial x_j} + \eta c e_j\right] \tag{8}$$

where $D_{ij} = \emptyset\bar{D}_{ij}$, $\bar{D}_{ij}$ is dispersion tensor, V_i is Darcy velocity vector, c^+ is solute concentration of infection or drilling, and K_{ij}^0 is the hydraulic conductivity at the reference (freshwater) condition.

The initial and boundary conditions of the flow equations were described as follows:

$$\text{Boundary } B_1 : \begin{cases} h(x_i, 0) = h_0(x_i) \\ h(x_i, t) = \hat{h} \end{cases} \tag{9}$$

$$\text{Boundary } B_2 : V_i n_i = -V_n \tag{10}$$

where h_0 is the initial head, $\hat{h}$ is prescribed head, n_i is the outward unit normal vector, and V_n is prescribed fluid flux, which is positive for inflow and negative for outflow.

Initial and boundary conditions for solute transport are described as below:

$$\text{Boundary } B_1' : \begin{cases} c(x_i, 0) = c_0 \\ c(x_i, t) = \hat{c} \end{cases} \tag{11}$$

$$\text{Boundary } B_2' : D_{ij}\frac{\partial c}{\partial x_j}n_i = q_c^D \tag{12}$$

$$\text{Boundary } B_3' : D_{ij}\frac{\partial c}{\partial x_j}n_i - V_i n_i c = q_c^T \tag{13}$$

where c_0 is initial concentration, $\hat{c}$ is the prescribed concentration of Boundary B$'_1$, q_c^D is the dispersive mass flux of solute of Boundary B$'_2$, and q_c^T is the total mass flux of solute in which q_c^D and q_c^T are positive for inward mass flux and negative for outward mass flux.

In this study, the FEFLOW model was adopted to simulate the results from the experiments. Groundwater flow and solute transport simulation software FEFLOW developed by Berlin Water Resources Planning and System Research Institute was used to solve the mathematical model. The phreatic aquifer is the target layer in this study. The length and height of the simulation zone are 1600, 370 mm, respectively. The top boundary is free surface, and the bottom is the impermeable boundary. The left side is seen as freshwater with concentration 0 mg/L, and the right side is seen as salt water with concentration 25,000 mg/L. The constant head of the left side and the right side is 340 and 370 mm, respectively. It is splitted into 486 units and 494 nodes.

The horizontal permeability coefficient is 2.2×10^{-3} m/s, the vertical permeability coefficient is 2.2×10^{-4} m/s, the horizontal and vertical dispersion value was 0.0083 and 0.00083 m, respectively, and porosity is 32.86%. The seepage control board was used to simulate subsurface barriers. The height of the board is 600 and 280 mm far away from the saltwater area. The permeability coefficient of subsurface barriers is 9.9×10^{-7}, 1.3×10^{-7} and 3.7×10^{-8} m/s, respectively.

3 Results and discussion

3.1 No barriers

The results of sandbox test and numerical simulation were compared when the saltwater migrated for 10, 20 and 40 min (Fig. 2). The left side is treated as a reference head as
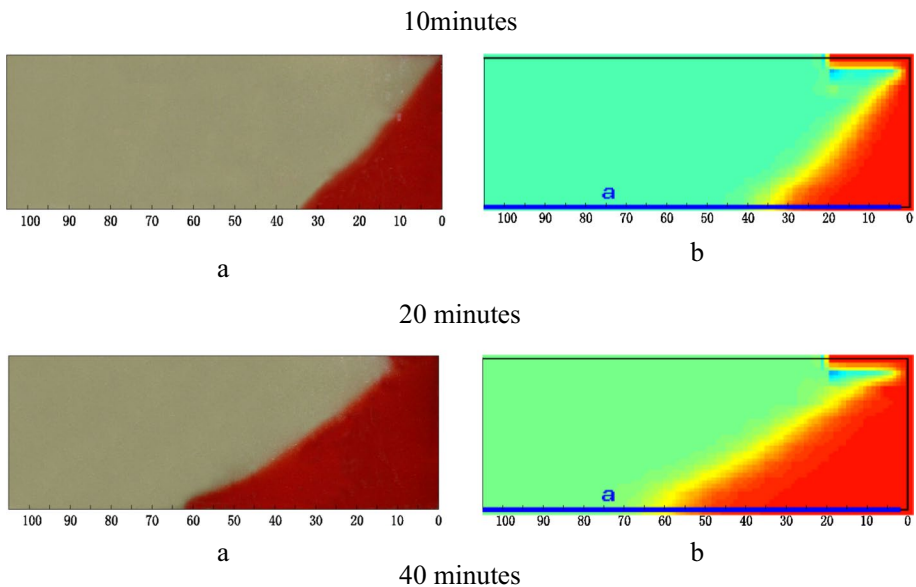
Fig. 2 Comparison of experimental and simulation results without subsurface barrier

0 mm, while the right side is treated as a reference head which increased from 0 to 30 mm with the increase in depth. Saltwater concentration of the right side was 25000 mg/L. Figure 2a is the result of the physical model, and Fig. 2b is the numerical simulation result.

When the experiment time was 10, 20 and 40 min, the migration distance of saltwater front in sandbox test was 18, 35 and 63, respectively, while in numerical simulation it was 20, 35, 64 cm when the salt–fresh water interface migration time was 10, 20 and 40 min, respectively.

3.2 Semipermeable barriers

The semipermeable barriers were set up with two permeability coefficients, $K = 9.9 \times 10^{-7}$ m/s and $K = 1.3 \times 10^{-7}$ m/s, the sandbox test results of the two permeability coefficients are shown in Fig. 3 and the simulation results are shown in Fig. 4.

There was difference in the simulation results between the two permeability coefficients subsurface barriers. For $K = 1.3 \times 10^{-7}$ m/s, when the experiment time was within 20 min,
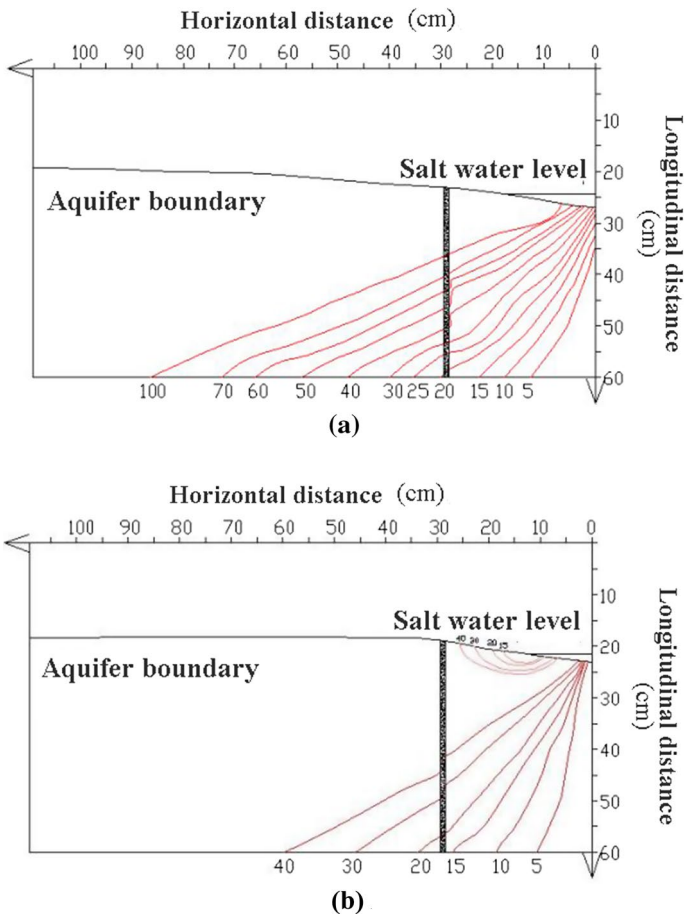
Fig. 3 The sandbox test results when the hydraulic conductivity was 9.9×10^{-7} and 1.3×10^{-7} m/s. **a** $K = 9.9 \times 10^{-7}$ m/s, **b** $K = 1.3 \times 10^{-7}$ m/s
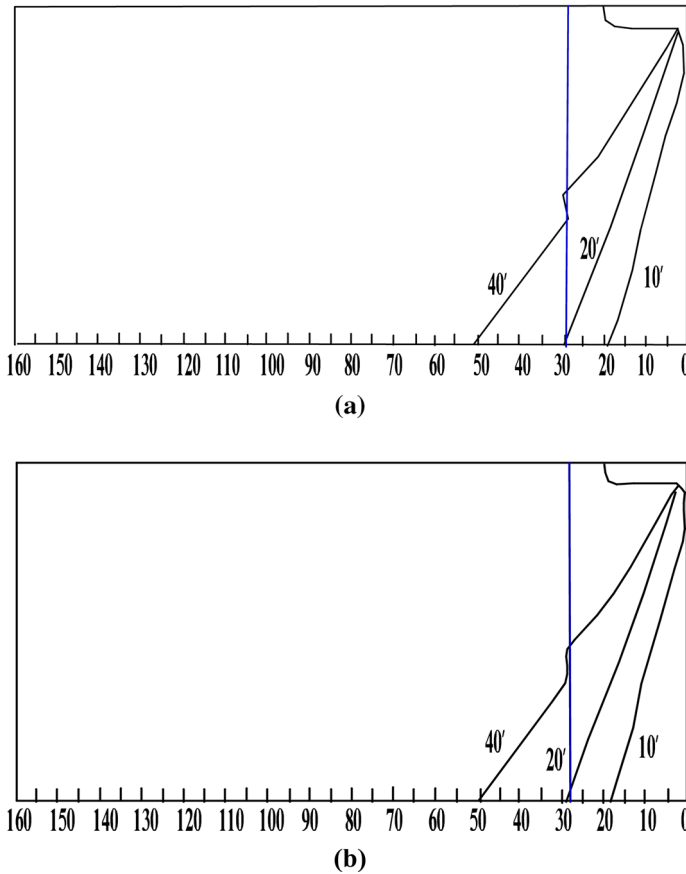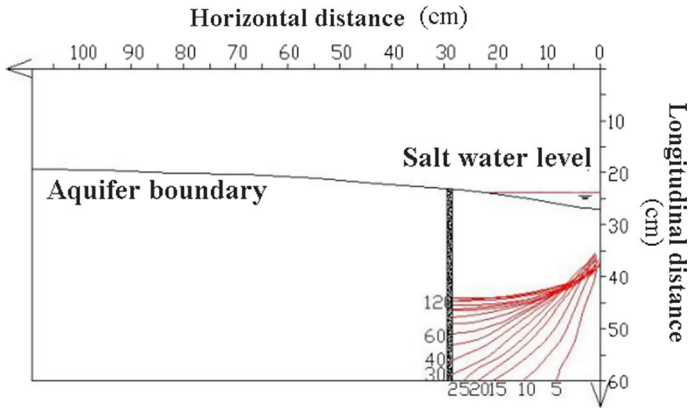
Fig. 4 Numerical simulation results when the hydraulic conductivity was 9.9×10^{-7} and 1.3×10^{-7} m/s. **a** $K = 9.9 \times 10^{-7}$m/s, **b** $K = 1.3 \times 10^{-7}$m/s

the saltwater front did not pass though the barrier, and shape of salt–fresh interface was not changed significantly, but 40 min later, the salt water front went through the subsurface barriers, and the salt–fresh water interface morphology was changed. When the salt water passed through the subsurface barrier, the migration rate of the salt–fresh water interface was obviously lower than before. It showed that the subsurface barrier could effectively reduce the migration rate of the salt–fresh water interface. It could be seen that when the experiment was carried out in 40, 50 and 60 min, there was an emergence of broken line in the interface between the salt–fresh interface and the subsurface barriers. The migration rate decreased when the saltwater passed through the subsurface barriers, which indicated that the subsurface barrier had a certain interception effect on saltwater intrusion. However, when in 70 min, the salt–fresh interface migration rate was the same before and after the subsurface barrier, with the time going on, the effect of subsurface barriers on saltwater intrusion was less significant.

It can be seen in Fig. 7a that the results of numerical simulation and experimental results were basically identical, which indicated that the model could simulate the saltwater intrusion well when there were subsurface barriers.

Fig. 5 The sandbox test results when the hydraulic conductivity was 3.7×10^{-8} m/s
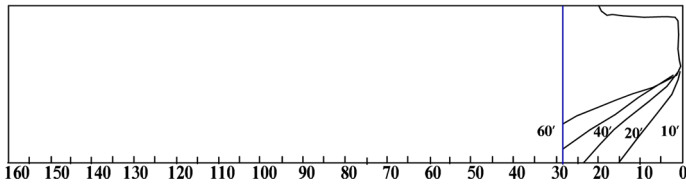

Fig. 6 Numerical simulation results when the hydraulic conductivity was 3.7×10^{-8} m/s

3.3 Impermeable barriers

The subsurface barrier can be seen as impermeable barrier when the hydraulic conductivity is 3.7×10^{-8} m/s. The sandbox test results and the numerical simulation results under this condition are shown in Figs. 5 and 6.

From the simulation results, we could see that the invasion of saltwater did not pass through the subsurface barriers. It could also be seen from the experimental results that migration rate of salt–fresh water interface reduced greatly when the permeability coefficient was smaller than 10^{-8} m/s, which indicated the subsurface barriers could prevent saltwater intrusion effectively. As larger density, the saltwater mainly distributed in the lower part of the porous medium. The salt water in the upper was gradually desalinated with migration.

Then we compared the experimental results and numerical simulation results of no barriers and with different barriers, the fitting results are shown in Fig. 7a–d. It can be seen in Fig. 7a–d that the results of numerical simulation and experimental results were basically identical, which indicated that the model could simulate the saltwater intrusion well when there were subsurface barriers and there were not subsurface barriers.
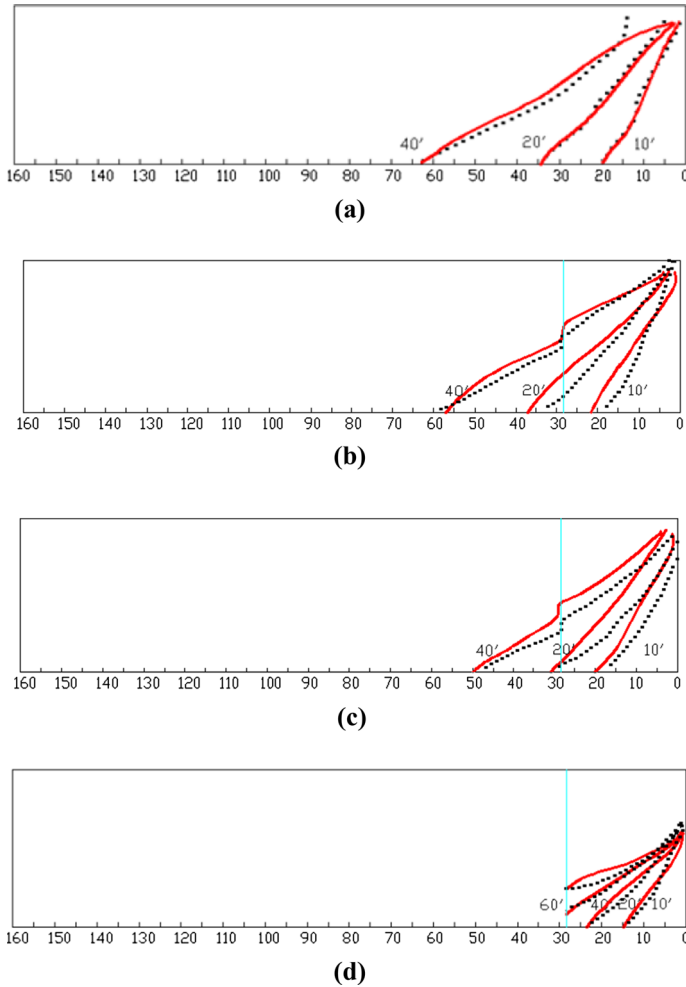
Fig. 7 The fitting results of the saltwater intrusion simulation with and without subsurface barriers. **a** Without subsurface barrier, **b** $K = 9.9 \times 10^{-7}$ m/s, **c** $K = 1.3 \times 10^{-7}$ m/s, **d** $K = 3.7 \times 10^{-8}$ m/s

4 Discussion

The influence of the subsurface barriers with different permeability coefficients on the salt-water intrusion rate could be analyzed from the concentration variation of the observation point. Concentration variation with time of observation point in different permeability coefficients subsurface barriers is shown in Fig. 8.

There was difference for the concentration variation of the observation point with and without subsurface barriers. The concentration of observation point increased rapidly and reached saturation in less than half an hour without subsurface barrier, which indicated that the salt water migrated to the observation point in less than half an hour. With the decrease in the permeability coefficient of subsurface barriers, the time to saturate the observation
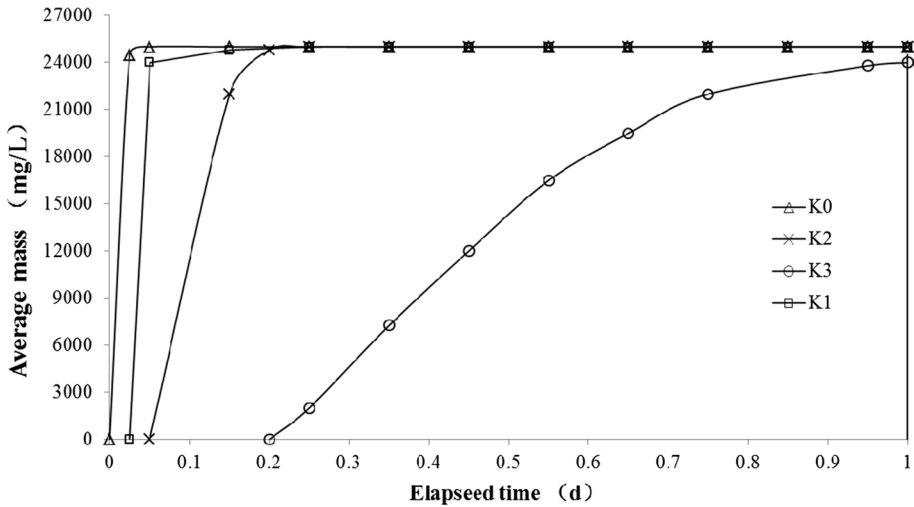
Fig. 8 Concentration variation curves of observation point. Note: K0 represents no subsurface barrier; K1 represents the permeability coefficient of subsurface barrier is 9.9×10^{-7} m/s; K2 represents the permeability coefficient of subsurface barrier is 1.3×10^{-7} m/s; K3 represents the permeability coefficient of subsurface barrier is 3.7×10^{-8} m/s

point gradually increased. It took about 1 hour for salt water to migrate to the observation point when the K was 10^{-6} m/s, which indicated that it had little effect to prevent the saltwater intrusion when the hydraulic conductivity of subsurface barriers was larger than 10^{-6} m/s. When the K was 10^{-7} m/s, the salt water migrated to the observation point in about 4.5 h, which indicated that the subsurface barriers had a certain effect to prevent the saltwater intrusion. When the K decreased to 10^{-8} m/s, the concentration variation curve was different with other curves. It increased very slowly and did not reach saturation in the final, which indicated that the salt water was almost not go through the subsurface barriers.

Fig. 9 Salt–fresh water interface migration distance with time
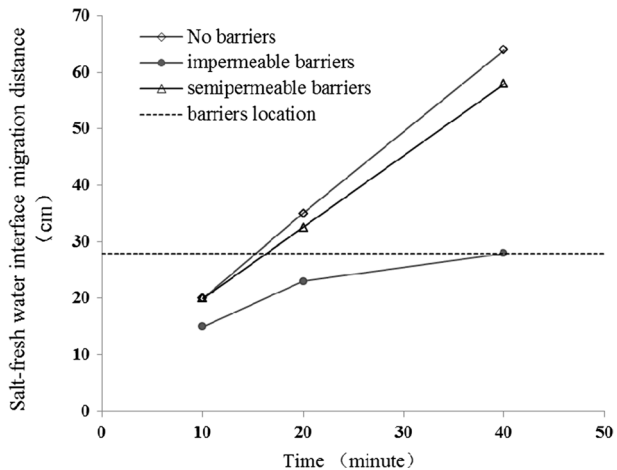
Therefore, it had an obvious restraining effect on the saltwater intrusion when the K of the subsurface barriers was less than 10^{-8} m/s.

Then, the salt–fresh water interface migration distance with time was different without subsurface barrier ($K = 2.2 \times 10^{-3}$ m/s) and with subsurface barriers that $K = 9.9 \times 10^{-7}$ and $K = 3.7 \times 10^{-8}$ m/s. We could see from Fig. 9 that the salt–fresh water interface migration distance with no barriers ($K = 2.2 \times 10^{-3}$ m/s) was longer than that with semipermeable barriers ($K = 9.9 \times 10^{-7}$ m/s), and the migration distance was the shortest with impermeable barriers ($K = 3.7 \times 10^{-8}$ m/s) when the migration time was the same. With time going, the difference in salt–fresh water interface migration distance between no barriers and semipermeable barriers and impermeable barriers became larger. When it was in 40 min, the salt–fresh water interface migration distance was no longer increasing, which indicated that the salt water cannot go through the barriers. The salt–fresh water interface migration distance increased linearly with time increasing when without subsurface barriers and with semipermeable barriers, while it increased in logarithmic with time increasing when with impermeable subsurface barriers.

From the discussions above, we could see that it had no effect on saltwater intrusion when the hydraulic conductivity was larger than 10^{-3} m/s, while it could well prevent the seawater intrusion when the hydraulic conductivity was less than 10^{-8} m/s. This meas that low permeability of subsurface barriers has good effectiveness of mitigation of saltwater intrusion. It is the reason that the grouting cement is often used as subsurface barrier materials in the engineering practice in China.

5 Conclusions

(a) The dynamic changes of the salt–fresh water interface with and without subsurface barriers were simulated through laboratory sandbox test by coloring technology, image processing technology and water quality testing technology. Results showed that with migration time increasing, the saltwater intrusion rate decreased till to maintain an equilibrium state of salt–fresh water interface when without subsurface barriers. When the subsurface barriers induced, the lower the hydraulic conductivity of barriers, the more significant the interception effect of the subsurface barriers. The subsurface barriers could effectively prevent the intrusion of saltwater when the permeability coefficient was less than 10^{-8} m/s.

(b) According to the laboratory sandbox test, through artificial parameters adjusting, saltwater intrusion numerical simulation was carried out using FEFLOW model. Results showed that the laboratory sandbox test results and the numerical simulation results were fitted very well. At the same time, the longitudinal dispersion, transverse dispersion, permeability coefficient and other parameters were determined which could provide basis for establishing a three-dimensional saturated medium, unsteady flow and transient solute transport model and simulating large-scale saltwater intrusion process. In addition, sandbox model which was used to simulate saltwater intrusion revealed the mechanisms and process of saltwater intrusion and provided theoretical basis for the prevention and control of saltwater intrusion.

References

Abarca E, Carrera J, Sánchez-Vila X et al (2007) Quasi-horizontal circulation cells in 3D seawater intrusion. J Hydrol 339(s3–4):118–129

Abd-Elhamid HF, Javadi AA (2011) A cost-effective method to control seawater intrusion in coastal aquifers. Water Resour Manage 25(11):2755–2780

Allow KA (2012) The use of injection wells and a subsurface barrier in the prevention of seawater intrusion: a modelling approach. Arab J Geosci 5(5):1–11

Chekirbane A, Tsujimura M, Kawachi A et al (2015) 3D simulation of a multi-stressed coastal aquifer, northeast of Tunisia: salt transport processes and remediation scenarios. Environ Earth Sci 73:1427–1442

Chen HH, Wang XM, Zhang YX et al (2000) Three-dimensional numerical simulation and analysis of sea-salt water intrusion dynamic system in the lower reaches of Weihe River. Earth Sci Front 7:297–304

Cheng JM (1999) Coastal seawater intrusion in the multilayer aquifer system three dimensional water quality model and application. China university of Geosciences

Cobaner M, Yurtal R, Dogan A et al (2012) Three dimensional simulation of seawater intrusion in coastal aquifers: a case study in the Goksu Deltaic Plain. J Hydrol 464–465(2):262–280

Galeati G, Gambolati G, Neuman SP (1992) Coupled and partially coupled Eulerian–Lagrangian model of freshwater-seawater mixing. Water Resour Res 28(1):149–165

Guo W, Bennett GD (1998) SEAWAT version 1.1: a computer program for simulation of groundwater flow of variable density. Missimer International Inc, Fort Myers

Guo W, Langevin CD (2002) User's guide to SEAWAT: a computer program for simulation of three-dimensional variable density groundwater flow: techniques of water-resources investigations book 6, Chapter A7, p 77 (Supersedes OFR 01-434)

Huyakorn PS, Jones BG, Parker JC, Wadsworth TD, White HO (1987) Finite element simulation of moisture movement and solute transport in a large caisson. In: Springer EP, Fuentes HR (eds) Modeling study of solute transport in the unsaturated zone, Los Alamos National Laboratory U.S. NRC, NUREG/CR-4615, pp 117–170

Li GM, Chen CX (1995) WeiZhou island seawater intrusion simulation. Hydrogeol Eng Geol (5):1–5

Lin HJ, Rechards, Talbot CA et al (1997) A three-dimensional finite-element computer model for simulating density-dependent flow and transport in variable saturated media: version 3.1. US Army Engineering Research and Development Center, Vicksburg

Lu W, Yang QC, Martín JD et al (2013) Numerical modeling of seawater intrusion in Shenzhen (China) using a 3D density-dependent model including tidal effects. J Earth Syst Sci 122(2):451–465

Rumer RR, Harleman DRF (1963) Intruded salt-water wedge in porous media. J Hydraul Div 86:192–220

Tang J, Lv XB, Yu CZ (1998) Experimental investigation the mechanisms of freshwater-saltwater transition zone in groundwater. J Tsinghua Univ 38:63–66

Todd DK (1980) Saline water intrusion in aquifers in groundwater hydrology [M]. Wiley, pp 494–517

Wu JC, Xue YQ, Xie CH et al (1996) Water-rock interaction cation exchange in the process of sea water intrusion. Hydrogeol Eng Geol (3):18–19

Yuan Y, Liang D (2001) Afterwards prediction of seawater intrusion and controlling engineering. Appl Math Mech 22(11):163–171

Zhang Q (2005) An experimental study of seawater intrusion. Hydrogeol Eng Geol 32(4):43–47

Zhang W, Ying H, Yu X et al (2015) Multi-component transport and transformation in deep confined aquifer during groundwater artificial recharge. J Environ Manage 152:109–119

Zhao J, Jin L, Wu JF et al (2016) Numerical modeling of seawater intrusion in Zhoushuizi district of Dalian City in northern China. Environ Earth Sci 75(9):1–18